Linear stability and instability patterns in ion-sputtered silicon

2009 J. Phys.: Condens. Matter 21 224010

(http://iopscience.iop.org/0953-8984/21/22/224010)

IOP Publishing Journal of Physics: Condensed Matter

J. Phys.: Condens. Matter **21** (2009) 224010 (8pp) doi:10.1088/0953-8984/21/22/224010

Linear stability and instability patterns in ion-sputtered silicon

Charbel S Madi, H Bola George and Michael J Aziz

Harvard School of Engineering and Applied Sciences, Cambridge, MA 02138, USA

Received 24 February 2009
Published 12 May 2009
Online at stacks.iop.org/JPhysCM/21/224010

Abstract

We study the patterns formed on Ar^+ ion-sputtered Si surfaces at room temperature as a function of the control parameters ion energy and incidence angle. We observe the sensitivity of pattern formation to artifacts such as surface contamination and report the procedures we developed to control them. We identify regions in control parameter space where holes, parallel mode ripples and perpendicular mode ripples form, and identify a region where the flat surface is stable. In the vicinity of the boundaries between the stable and pattern-forming regions, called bifurcations, we follow the time dependence from exponential amplification to saturation and examine the amplification rate and the wavelength in the exponential amplification regime. The resulting power laws are consistent with the theory of nonequilibrium pattern formation for a type I (constant wavelength) bifurcation at low angles and for a type II (diverging wavelength) bifurcation at high angles. We discuss the failure of all sputter rippling models to adequately describe these aspects of the simplest experimental system studied, consisting of an elemental, isotropic amorphous surface in the simplest evolution regime of linear stability.

(Some figures in this article are in colour only in the electronic version)

1. Introduction

Uniform ion beam sputter erosion often causes a spontaneously arising pattern of corrugations, holes or dots [1]. Periodic self-organized patterns with spacings as small as 7 nm [2] have stimulated interest in this method as a means of sub-lithographic nanofabrication [3]. We are studying spontaneous pattern formation in uniform noble-ion irradiation of silicon. Due to its simplicity, this system is a very promising one for using in experiments as a rigorous test of theory: it is a monatomic system amenable to molecular dynamics (MD) simulation and its surfaces are amorphous under ion bombardment, thereby minimizing potentially confounding effects of disproportionation and crystallographic singularities. If theory and experiment cannot agree in such a prototypical simple system as this, where can they possibly agree? And if we cannot make them agree even in the linear regime of exponential amplification, how much confidence can we have in the results of explorations of patterns evolving from nonlinear terms as they are added to the wrong linear partial differential equation (PDE)?

In the linear stability theory of Bradley and Harper [4] (BH) the pattern originates from different wavenumber dependences of the destabilizing (roughening) effect in which the erosion rate is enhanced at regions of high concave curvature and the stabilizing (smoothening) effect of surface diffusion. Whereas BH theory explains several experimental observations, significant contradictions are evident. Several of these are attributable [1] to crystallographic effects missing from BH, but the most serious ones are those occurring on amorphous surfaces, for which BH was designed. One particularly important prediction of BH is that a flat surface is unstable to perpendicular mode ripples (wavevector perpendicular to the ion beam) under uniform ion irradiation at any incidence angle. Another is that the dominant instability undergoes a 'ripple rotation' from parallel mode (wavevector parallel to the projected ion beam) near normal incidence to perpendicular mode near grazing incidence. The trend that emerges from a number of studies on amorphous surfaces such as quartz glass [5] and room-temperature silicon [6–9] is ripple rotation at high angles (which is qualitatively consistent with BH) but a transition to a stable flat surface at low or intermediate angles (which is inconsistent with BH). It is possible that, because the sputter yield is highest near the angles where ripple rotation is observed, the erosive component (perhaps adequately modeled by the Gaussian ellipsoids in BH, discussed below) of the surface response dominates over the component from local mass redistribution [6, 10, 11]. In making this comparison with experiment, two caveats should be kept in mind. First, these

experimental studies are often of saturated structures after high fluence, and their relation to the dominant linear instability is not always clear. And second, the difficulty of concluding that a flat surface enjoys stability is that care must be taken to distinguish experimentally between truly stable flat surfaces and surfaces that are undergoing amplification of an instability at rates too low to be measured.

In this work we concern ourselves with the prediction of BH that a flat, uniformly irradiated surface is always unstable and compare it to experimental ranges of two control parameters—incident angles θ and ion beam energies E—where the surface is stable. We take care to identify and confine our attention to the 'linear regime' of exponential amplification at early time and low fluence. Sharp boundaries between stable and unstable regimes in control parameter space are known as *bifurcations*. Nonequilibrium pattern formation theory predicts that near bifurcations pattern features are universal, depending only on general characteristics of the dynamics, such as its symmetries, degree of criticality (i.e. whether the amplitude vanishes continuously or discontinuously), and whether the characteristic length scale vanishes, diverges or remains finite at bifurcation [12]. We carried out a careful characterization of patterns around bifurcation points by varying both incidence angle and ion beam energy in room-temperature Si bombardment [13]. We found that this monatomic, isotropic system exhibits two different types of supercritical bifurcations as incidence angle and ion energy are varied: at low θ a bifurcation of type I, characterized by constant wavelength, and, at high θ, another bifurcation, of type II, characterized by diverging wavelength [12]. Supplemented by analysis of evolving patterns near and away from bifurcations, this observation leads us to conclude that no existing theory is adequate for this monatomic, isotropic system, even at early times when nonlinear terms may be neglected.

This paper is organized as follows. In section 2, the experimental details are discussed. The experimental results, section 3, contain two subsections. The sensitivity of pattern formation to artifacts such as metal incorporation coming from the ion gun and sample surroundings together with the procedures developed to control the surface contamination are presented in section 3.1. In section 3.2, we compile our results into a phase diagram of pattern versus the control parameters E and θ which is characterized by supercritical bifurcations of type I (constant wavelength) and type II (diverging wavelength). In section 4, we discuss the various possible scenarios that can account for the observed empirical results. The dependence of the amplification rate and wavelength on the control parameters is consistent with the theory of pattern formation outside of equilibrium. Finally, the conclusions are presented in section 5.

2. Experiment

We performed argon ion (Ar^+) irradiation experiments on 1 cm^2 Si(001) square samples (p type, 1–10 Ω cm) in an ultra-high vacuum chamber (base pressure 7×10^{-11} Torr at room temperature) with the projected ion beam direction along the [110] crystallographic direction. The argon ions were generated using a 3 cm RF source with graphite accelerating grids[1]. The ion flux from the source was 0.57 mA cm^{-2} in the plane perpendicular to the ion beam. The beam divergence was roughly 4.5° and the distance to the target was approximately 15 cm. To vary the incidence angle samples were fixed, using melted indium, onto graphite wedges of various angles which were shielded everywhere from the ion beam by Si wafer shields. Thus, only silicon was exposed to the direct ion beam and contamination-induced dynamics is suppressed [14]. Energy-dispersive x-ray spectroscopy (EDXS), x-ray photoelectron spectrometry (XPS) and a scanning tunneling electron microscopy (STEM) map scan were employed to assess the surface impurity coverage of some of the Si samples after the completion of ion sputtering. The only elements that were evident were Si, O, Ar and C, and the O and C signals from the ion beam sputtered samples were indistinguishable from those from a Si wafer taken directly out of the box.

3. Results

3.1. Effect of surface contaminants on ion sputter erosion surface morphology

During the course of these studies we noticed that pattern formation on Ar^+ ion-sputtered Si surfaces at room temperature is extremely sensitive to the experimental configuration. Important factors include the manner in which the Si samples are fixed to the substrate holder within the vacuum chamber, the grid material and the alignment of the grids within the ion gun.

In many ion beam sources such as ours, the screen grid (the first grid traversed by the ions) determines the ultimate kinetic energy and the accelerating grid (the second grid traversed) determines the divergence of the extracted ions. Ziberi *et al* [15] have reported the sensitivity of pattern formation to the voltage of the accelerating grid at constant kinetic energy. They interpret this observation as a sensitivity to beam divergence; in principle, the fundamental sensitivity is presumably to the 'convergence'—i.e. the distribution of incoming angles at a point on the sample surface—which is related to, but can be different from, the divergence. We recently noticed a sensitivity to the mechanical alignment of the grid openings themselves as an apparent shift in the boundary between 'holes' and 'perpendicular mode ripples' in the phase diagram of figure 5. At 250 eV, 5° from normal incidence, 20 min exposure, before the graphite grids were realigned we observed holes and dots whereas after realignment we observed perpendicular mode ripples under nominally identical conditions. Consequently, in figure 5, for which all the data reported were taken prior to grid realignment, we have placed the boundary between holes and perpendicular mode ripples to lie at 5°, reflecting an uncertainty in boundary position associated with grid alignment. In fact, there may be no sharp boundary, but rather a continuum of morphologies between 'holes' and

[1] Veeco, Fort Collins, CO.

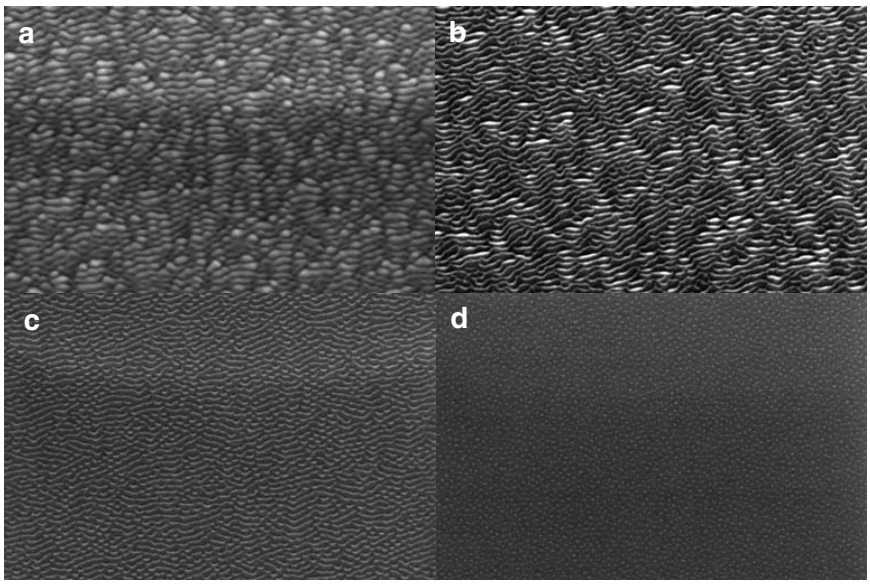

Figure 1. Effect of molybdenum (Mo) clips on surface morphology following irradiation with 250 eV Ar^+, 30° off-normal incidence, and fluence of 6.4×10^{18} Ar^+ cm^{-2} using graphite grids. (a)–(d) display scanning electron microscopy (SEM) images within 1 μm of the edge of the Mo clips, and 50 μm, 100 μm and 1000 μm away from the clips, respectively. The projected ion beam runs from the bottom of the page to the top. The clip edge is located just off the left edge in (a), running vertically. The SEM scan size is 1.5 μm × 1.125 μm.

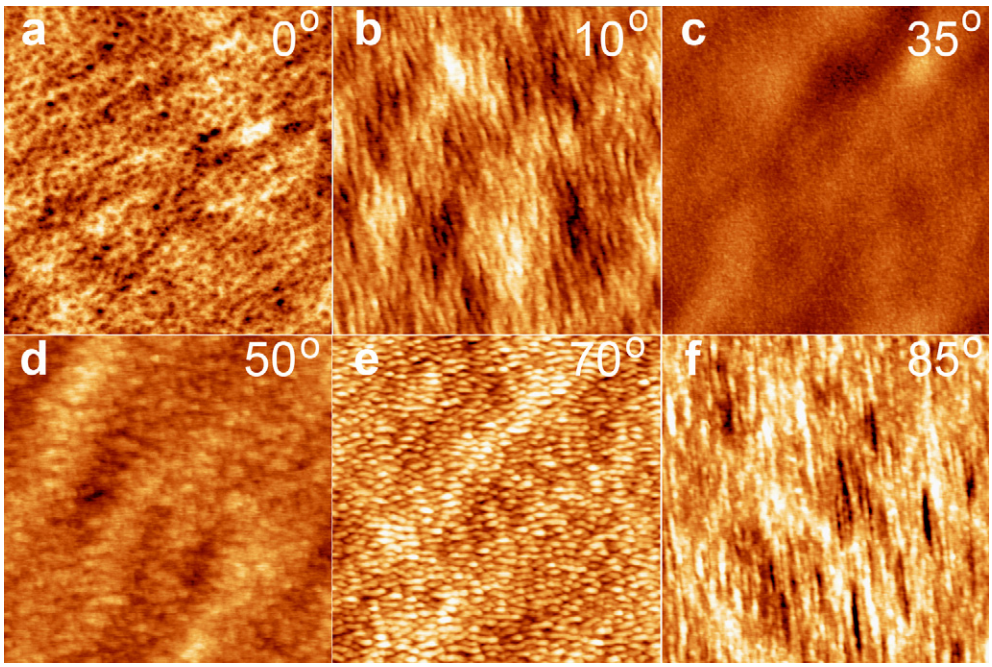

Figure 2. Effect of incidence angle on surface morphology following irradiation with 250 eV Ar^+ at room temperature. In all cases, the projected ion beam runs from the bottom of the page to the top. The AFM topograph scan size is 2 μm × 2 μm in (a)–(c) and 1 μm × 1 μm in (d)–(f). (a) 0°, 3.8×10^{18} Ar^+ cm^{-2} (18 min), vertical range 3 nm. (b) 10°, 18 min, vertical range 3 nm. (c) 35°, 18 min, vertical range 3 nm. (d) 50°, 3.2×10^{17} Ar^+ cm^{-2} (90 s), vertical range 2 nm. (e) 70°, 90 s, vertical range 3.5 nm. (f) 80°, 90 s, vertical range 3.5 nm.

'perpendicular mode ripples': the topographic pattern at 10° in figure 2(b) may be interpreted as 'holes' that are stretched along the direction of the projected ion beam.

Ion bombardment of Si samples fixed in the vacuum chamber using Mo clips that are directly exposed to the ion beam resulted in an array of dots inhomogeneously distributed on the sample surface, no matter whether graphite (C) or molybdenum (Mo) grids were used. High densities of dots developed immediately adjacent to the clips, forming a ripple-like structure, with a gradual transition to an isotropic distribution of dots ∼1 mm from the clips, as shown in figure 1. In contrast, fixing the substrate to the holder using melted indium (with no indium exposed to the ion beam) and without using any clips resulted in a featureless steady-state surface

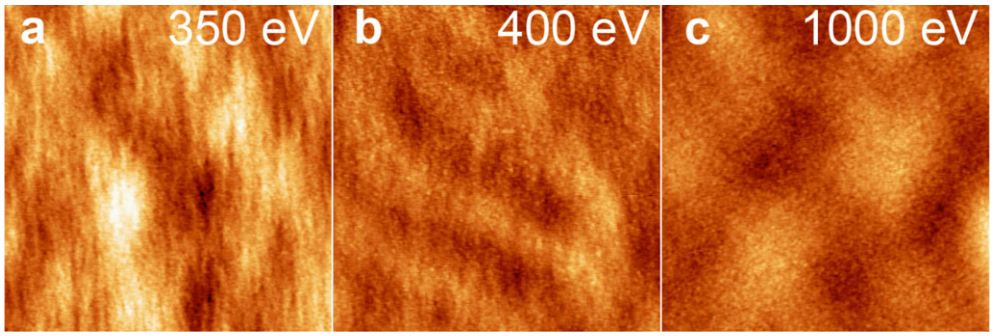

Figure 3. Effect of ion energy on surface morphology following irradiation at 10° from normal incidence at room temperature. In all cases, the ion fluence is 3.8×10^{18} Ar^+ cm^{-2} (18 min), the projected ion beam runs from the bottom of the page to the top, the AFM topograph scan size is 2 μm × 2 μm and the vertical range is 2 nm. The image in figure 2(b) may be considered to be the first image in this sequence.

under otherwise identical irradiation conditions using graphite grids. Hence, it appears likely that trace metal contamination from the Mo grids and clips is directly responsible for the dot pattern formation, which extends over the entire 1 × 1 cm^2 Si surface. Similar observations of the sensitivity of pattern formation to surface metal content were reported by Ozaydin *et al* [14], who used Mo clips to fix their samples and reported XPS measurements indicating Mo concentrations of 5–15%; and by Sanchez-Garcia *et al* [16], who measured by Rutherford backscattering spectrometry (RBS) about 5% of Mo and Fe combined in their samples arising from the Mo clips and the cold cathode ion source, respectively. We examined some of our irradiated silicon surfaces for surface contamination using RBS and XPS. For a series of specimens that were directly contacted by silicon clamps, which themselves were held down by Mo clips, and with no direct line of sight from any of the irradiated Mo clips or graphite sample holder material to the sample surface, RBS measurements indicated an Mo surface coverage of $1–9 \times 10^{14}$ cm^{-2} on specimens irradiated using Mo grids at 150–500 eV for 30 min at 10° from normal incidence. Ion bombardment of an Mo-clipped silicon sample (with Si clamps) at 250 eV and 10° to a fluence of $4–8 \times 10^{18}$ cm^{-2} using C grids resulted in a distribution of dots superimposed on a ripple-like structure (e.g. figure 4(a)). XPS measurements on specimens irradiated with 4.2×10^{18} cm^{-2} at 10° and 250 eV revealed an apparent (not well-calibrated) atomic Mo concentration of about 2% when Mo clips and Si clamps had been used with either Mo or C grids. In contrast, when using graphite grids and no clips, a ripple-like structure with no dots formed, there was no XPS signal from any metal and the apparent concentration of carbon in the processed Si sample was indistinguishable from that in a new Si wafer taken directly out of the box. RBS is insensitive to C on Si and the sensitivity of XPS to carbon is less than that to molybdenum, and we are unable to put a reliable upper limit on the carbon coverage of our samples. However, we attribute the observed difference—between dots using Mo grids and Mo clips, and a featureless surface using graphite grids with no clips—to a trace metal contamination effect. In order to eliminate metal contamination we settled on graphite grids and clip-free indium soldering to a graphite substrate entirely shielded by silicon, as reported above, and for each kinetic energy we chose the voltage of the accelerating grid so as to minimize the beam divergence.

3.2. Type I (constant wavelength) and type II (diverging wavelength) bifurcations

Patterns for $\theta < 25°$ ($\theta > 45°$) were first observed at a fluence of $\sim 2 \times 10^{18}$ (1×10^{17}) cm^{-2}. The surface should become amorphous very quickly, after a fluence of the order of 10^{14} ions cm^{-2} [17]. A ∼3 nm amorphous surface layer was observed in cross-sectional TEM of samples irradiated at 250 eV and fluences exceeding 10^{17} cm^{-2} at angles exhibiting both instability and stability. In a control experiment at 250 eV and 10°, no difference was found between pattern development on a crystalline Si wafer and on a wafer pre-amorphized with an 80 keV Si^+ implant to a dose of 10^{16} cm^{-2} that resulted in an initial amorphous layer thickness of 192 nm.

After irradiation, AFM images were obtained from a Digital Instruments Nanoscope D3100 AFM in tapping mode. In figure 2 we show topographs of surfaces irradiated at room temperature by 250 eV Ar^+ at various incidence angles. Notably, at incidence angles near 35° the flat surface is stable under uniform ion sputter erosion. In figure 3 we show topographs of surfaces irradiated at room temperature at 10° from normal incidence with Ar^+ of varying kinetic energy. To further investigate the relative stability of the flat surface and the patterned surface, we started with a saturated rippled structure formed using 8×10^{18} Ar^+ cm^{-2}, 250 eV irradiation at $\theta = 10°$ and observed decay at all wavevectors upon further irradiation at 500 eV with the same dose, as shown in figure 4 [18]. This observation proves that the flat surface is truly stable, rather than unstable with an amplification rate too low to be detected.

In figure 5 we compile our observations into a phase diagram of pattern formed (or lack thereof) in the linear regime versus control parameter. Whereas at low θ we observe perpendicular mode ripples (wavevector perpendicular to the projected ion beam direction), at the high θ transition to instability we see parallel mode ripples (wavevector parallel to the projected ion beam). Finally, at sufficiently high θ we observe the perpendicular mode again. Several observations are qualitatively consistent with the phase diagram for 500–2000 eV Xe^+ irradiation of Si presented by Ziberi in his

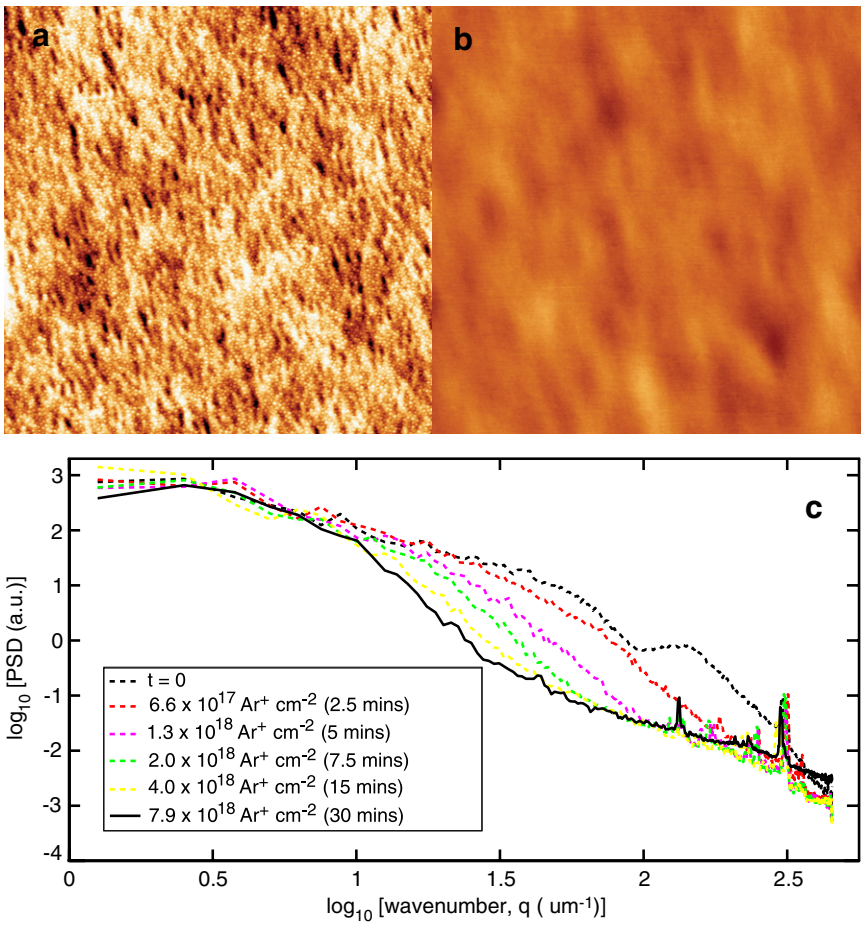

Figure 4. Top row: 5 μm $\times$ 5 μm AFM topographs of (a) a saturated rippled structure formed with 250 eV Ar^+, 10° off-normal incidence, ambient temperature and ion fluence of 8×10^{18} Ar^+ cm^{-2} (30 min at 0.7 mA cm^{-2}) and of (b) a stable flat surface obtained by irradiating sample in (a) with a fluence of 8×10^{18} Ar^+ cm^{-2} at 500 eV Ar^+ and 10° off-normal incidence. The projected ion beam runs from the bottom of the page to the top and the vertical range is 7 nm in both images. Second row: time sequence of 1D circularly averaged power spectral densities (PSDs) resulting from ion bombarding sample starting with the configuration shown in panel (a). The very high frequency peaks at $\sim \log_{10}[q(\mu m^{-1})] = 2.5$ are scanning artifacts from the AFM. Note that with increasing fluence both peaks centered at 125 μm^{-1}, corresponding to impurity-induced dots, and 56 μm^{-1}, corresponding to the saturated ripple structure, decay.

thesis [8], namely: an isotropic array of holes at normal incidence; a transition from holes to perpendicular mode ripples to flatness with increasing angle, and a transition from holes or perpendicular mode ripples to flatness with increasing energy at low angles. Other transitions, at higher energy or angle, appear to be sensitive to the particular system being studied.

We next focus on the bifurcation from a rippling instability to a stable flat surface as the control parameter (θ or E) traverses a critical value. To characterize this transition, we measured the RMS roughness and wavelength of the evolving pattern as the control parameter approaches the bifurcation point. In figure 6 we report the dependence of wavelength on θ and E as the bifurcation points are traversed. Two key features are apparent. As the low angle transition is approached in either θ or E, the wavelength remains practically constant[2]. At the high angle transition, the wavelength grows rapidly, apparently indicating divergence[3].

With figures 7 and 8 we focus on the pattern amplification near the bifurcation points. Figure 7(a) shows the RMS roughness versus time during irradiation at several angles near the high-θ bifurcation. We take this as a proxy for the amplification rate at the most unstable wavevector, which is readily predicted by most theories. We do this because we did not find an objective way of quantifying the amplification rate at the most unstable wavevector under the conditions of this study. We believe this is justified because, according to Parseval's theorem, the RMS roughness is the sum of the contributions from all the wavevectors in reciprocal space, and normally (with an exception noted below) we expect the Fourier components at and around the most unstable wavevector to dominate all contributions.

[2] We find the same qualitative behavior—a transition to a flat surface between 280 and 300 °C—as the temperature is raised at 10° off-normal incidence with ion energy 250 eV. We do not dwell on this case, however, because complications may arise involving a potentially decreasing degree of amorphousness of the surface with increasing temperature. Likewise, Gago *et al* [19] reported no divergence in the dot spacing of saturated Si structures at normal incidence as the transition to flatness is approached with increasing temperature.

[3] Similar behavior was reported in sapphire by Zhou *et al* [20].

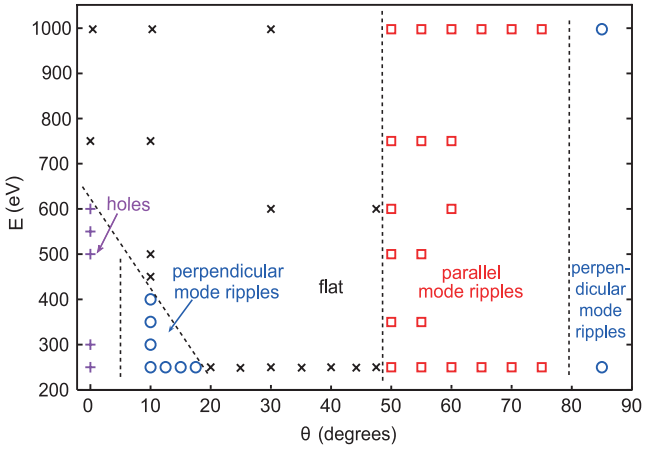

Figure 5. Phase diagram for linear regime of pattern formation versus control parameters θ and E. $\times$: flat; $+$: holes; circles: perpendicular mode ripples; squares: parallel mode ripples. Fluence is 3.8×10^{18} Ar^+ cm^{-2} except for ripples at $\theta \geqslant 50°$, where fluence is 3.2×10^{17} Ar^+ cm^{-2}.

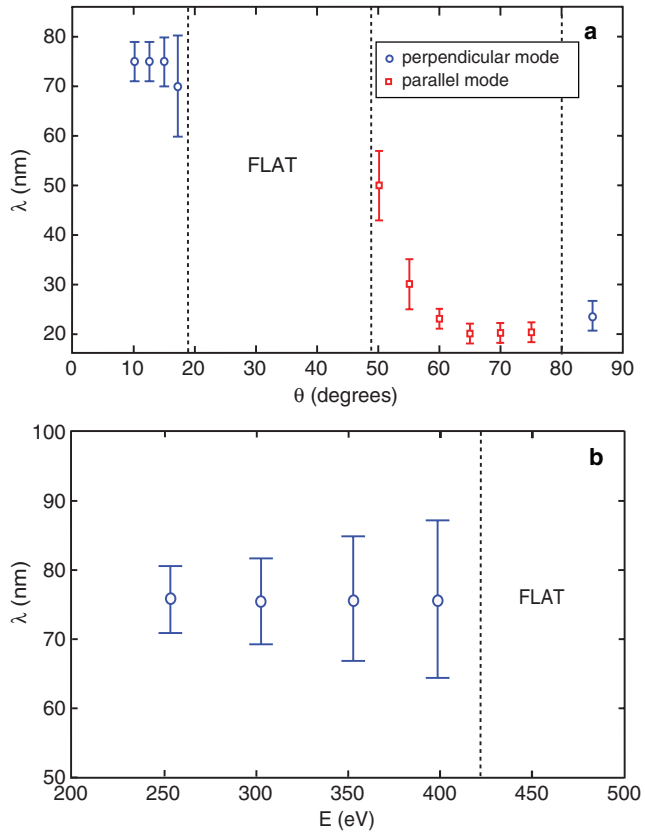

Figure 6. Ripple wavelength in the linear regime versus (a) θ at $E = 250$ eV; (b) E at $\theta = 10°$. Circles: perpendicular mode; squares: parallel mode.

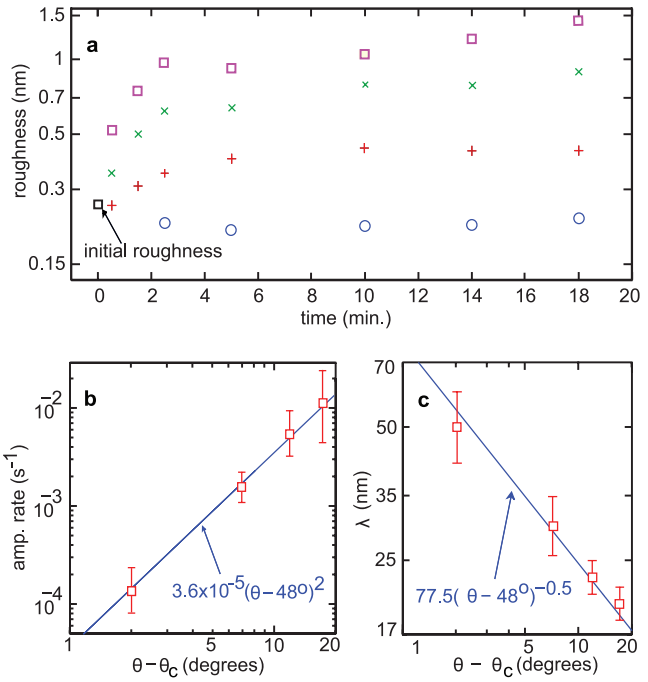

Figure 7. Behavior near bifurcation points for high-θ ripples at $E = 250$ eV. (a) Pattern amplitude (reckoned as RMS surface roughness) versus time. Squares: 65°; $\times$: 60°; $+$: 55°; circles: 50°. (b) Amplification rate versus misorientation for high-θ bifurcation, showing quadratic dependence. (c) Wavelength versus misorientation for high-θ bifurcation, showing inverse square root dependence.

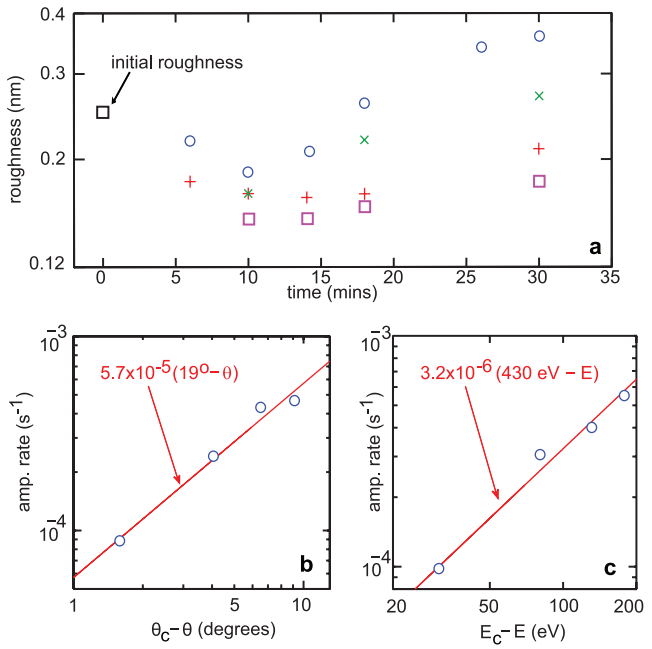

Figure 8. Behavior near bifurcation points for low-θ ripples. (a) Pattern amplitude (reckoned as RMS surface roughness) versus time, $E = 250$ eV. Squares: 17.5°; $+$: 15°; $\times$: 12.5°; circles: 10°. (b) Amplification rate versus misorientation, showing linear dependence, $E = 250$ eV. (c) Amplification rate versus E at $\theta = 10°$, showing linear dependence.

We observe saturation of the roughness after just a few minutes. Many studies have reported patterns observed well into the saturation regime, where nonlinear effects may be important. In order to safely neglect nonlinear effects, our measurements are restricted to the pre-saturation regime of exponential amplification, permitting us to directly test linear stability theories. Note that the roughness at $\theta = 50°$ initially decreases before beginning a slow rise. Our interpretation is that, out of the box, the silicon wafer's

roughness spectrum is not well matched to that amplified by the ion beam and that an initial transient period occurs wherein the 'wrong' Fourier components decay, eventually revealing the exponential amplification of the 'right' Fourier components. Figure 7(b) shows that the amplification rate varies quadratically with deviation from the high-θ bifurcation point. Figure 7(c) shows that the wavelength varies as the inverse square root of the misorientation. The power laws for the lines superposed on data are those expected for an infinite-wavelength bifurcation [12].

Figure 8(a) shows the RMS roughness versus time during irradiation at several angles near the low-θ bifurcation. We observe qualitatively similar amplification behavior as in the high-θ bifurcation (figure 7(a)) and offer the same interpretation, although the amplification rate here is slower and the initial transient lasts much longer and is observed over a wider range of angles. Figures 8(b) and (c) show that the amplification rate varies linearly with control parameter near the low-θ bifurcation point. The linear power law for the lines superposed on the data in figures 8(b) and (c) is that expected for a finite-wavelength (figures 6(a) and (b)) bifurcation [12].

The continuously vanishing amplification rate with control parameter indicates that all observed bifurcation points are supercritical. In the vicinity of supercritical bifurcations, pattern formation can be described by universal equations whose form depends only on general symmetries of the underlying dynamics and on the growth rate of the most unstable modes [12]. Hence any theoretical description of the patterns must agree with the global sequence of the experimentally identified bifurcations: finite-wavelength at low angles and diverging wavelength at high angles.

4. Discussion

Theories of sputter erosion predict a partial differential equation (PDE) for the evolution of a surface height profile $h(x; y; t)$. By assuming that the average response of the surface to the impact of a single ion is characterized by a cavity derived from Sigmund's Gaussian ellipsoid collision cascade model [21], BH derived the following PDE:

$$\frac{\partial h}{\partial t} = -I + \left\{ S_x \partial_{xx} + S_y \partial_{yy} - B\nabla^4 \right\} h, \qquad (1)$$

where $I(\theta)$ is the vertical erosion rate of a flat surface, $S_x(\theta)$ and $S_y(\theta)$ are its curvature coefficients, and B is a material parameter describing relaxation and containing the surface free energy and either the surface diffusivity or the viscosity of the ion-stimulated layer. A negative value of S_x or S_y leads to instability. BH showed that the Gaussian ellipsoid response implies $S_y < 0$ for all θ and E, i.e. a flat surface is unstable for some wavevector perpendicular to the ion beam. Regions of stability of a flat surface in our study, as well as several previous experimental studies of amorphous systems covering a sufficient range of incident angles to test this prediction, show it to be incorrect.

Modifications to the BH model have been proposed that allow stability for some range of incidence angles. Davidovitch *et al* [11] considered a modification of BH that results in replacing the BH curvature coefficients $S_x; S_y$ by effective coefficients S_x^{eff}, S_y^{eff}, whose control parameter dependence contains regimes where both coefficients are positive, implying stability of flat surfaces. These can arise either from response functions to ion impact with shapes different than Gaussian ellipsoids, or from ion-induced surface currents at the impact site as envisaged by Carter and Vishnyakov [6, 10]. With ion-induced surface currents as the only modification to BH theory, S_x^{eff} and S_y^{eff} can both be positive at low angles (i.e. stability, as we observe), with a sign change in S_x^{eff} occurring at intermediate angles [11] causing a parallel mode instability. For these models the pattern wavelength diverges at the bifurcation point [11]. This is a potential explanation of our observations at the high-θ bifurcation point at both high and low Ar^+ ion energy (figure 5) but cannot explain the behavior we observe at the low-θ bifurcation identified at low ion Ar^+ energy. Therefore the patterns formed at low angles and low ion energies must be caused primarily by a mechanism qualitatively different than those considered so far.

Davidovitch *et al* have argued that there are at least two ways for a bifurcation to occur with finite wavevector $\mathbf{q}$ (i.e. non-diverging wavelength) [11], such as we observe at low angle. Both of the ways identified so far involve non-local processes, requiring the introduction of integral operators whose range is much larger than the pattern wavelength. One way is by including the Facsko damping term $-K(h - \overline{h})$, where K is a positive constant [22, 23], and the average height $\overline{h}$ appears for consistency with translational invariance; this adds a constant term $-Kq^0$ to the linear dispersion relation. We note that the Facsko term was offered as a proxy for a model of redeposition but has not been derived from more fundamental principles. It is intriguing to note that Brown and Erlebacher found just such a $-Kq^0$ term when they measured the dispersion relation over a range of wavenumbers with positive amplification rate and fit it to a constant plus the BH dispersion relation (figure 9 of [24]). It is not possible to rule out effects of singular crystallographic energetics or kinetics because this measurement was performed on Si(111) at 733 °C, at which temperature the surface is almost certainly crystalline.

The other identified way to obtain a finite-wavelength bifurcation is by adding a $|\mathbf{q}|^3$ term due to ion-induced stress in the ion-stimulated surface layer. This additional destabilizing term causes the Asaro–Tiller (AT) elastic-energy-induced instability of solid surfaces [25, 26], and may become relevant if sufficient stress accumulates during the ion irradiation process [27, 28]. In this case the bifurcation occurs at finite q. The main problem with this mechanism is that preliminary *in situ* stress measurements [29] indicate stresses less than 200 MPa for which the standard ($S^{\text{eff}} = 0$) model [26] predicts an instability wavelength two orders of magnitude larger than that observed. Instabilities from a stress of this magnitude can work only if there is another (as yet unknown) mechanism for increasing its tenacity.

Another possible scenario, which we are currently investigating, is that the shape of the single-impact crater function varies from Sigmund's Gaussian ellipsoid response so as to change the relative stability of perpendicular and parallel mode at low angle (so that $S_y^{\text{eff}} < S_x^{\text{eff}} < 0$), while reversing their stability $S_x^{\text{eff}} < S_y^{\text{eff}}$ ($S_x^{\text{eff}} < 0$) at higher angles. In this form, the model would still predict diverging wavelengths at the bifurcation points. An additional process such as one of the non-local ones discussed above would still have to be significant in the vicinity of the finite-wavelength (low-θ) bifurcation.

5. Conclusions

We have examined stability and instability in the linear, exponential amplification regime for silicon surfaces. The phase diagram of pattern versus the control parameters E and θ exhibits regions of stability bordered by supercritical bifurcations of finite wavelength at low θ and diverging wavelength at high θ. The power laws observed for the amplification rate and the wavelength in the vicinity of these bifurcation points are consistent with those expected from the theory of nonequilibrium pattern formation. The BH theory is contradicted by the existence of the bifurcations as well as by the appearance, with increasing angle, of perpendicular mode before parallel mode ripples. The simplest modifications to the theory, such as the ion-induced surface current mechanism envisioned by Carter and Vishnyakov, are insufficient to explain the finite-wavelength bifurcation at low θ. It is surprising to find that, even in the linear regime for isotropic, elemental systems, at least one and quite possibly two additional physical effects beyond those in BH are necessary to explain the observed experimental results. A better understanding of the role of stress in the amorphous layer, a physical process leading to a non-local damping term, and the characterization of actual crater functions in physical experiments or MD simulations should be considered high research priorities.

Acknowledgments

This research was supported through DE-FG02-06ER46335. We thank Benny Davidovitch, Michael Brenner, Scott Norris and Bashkim Ziberi for helpful discussions.

References

[1] Chan W L and Chason E 2007 *J. Appl. Phys.* **101** 121301
[2] Wei Q, Lian J, Zhu S, Li W, Sun K and Wang L 2008 *Chem. Phys. Lett.* **452** 124–8
[3] Cuenat A, George H B, Chang K C, Blakely J and Aziz M J 2005 *Adv. Mater.* **17** 2845–9
[4] Bradley R M and Harper J M 1988 *J. Vac. Sci. Technol.* A **6** 2390
[5] Flamm D, Frost F and Hirsch D 2001 *Appl. Surf. Sci.* **179** 95–101
[6] Carter G and Vishnyakov V 1996 *Phys. Rev.* B **54** 17647–53
[7] Ziberi B, Frost F, Hoche T and Rauschenbach B 2005 *Phys. Rev.* B **72** 235310
[8] Ziberi B 2006 Ion beam induced pattern formation on Si and Ge surfaces *PhD Thesis* University of Leipzig
[9] Datta D P and Chini T K 2007 *Phys. Rev.* B **76** 075323
[10] Moseler M, Gumbsch P, Casiraghi C, Ferrari A C and Robertson J 2005 *Science* **309** 1545–9
[11] Davidovitch B, Aziz M J and Brenner M P 2007 *Phys. Rev.* B **76** 205420
[12] Cross M C and Hohenberg P C 1993 *Rev. Mod. Phys.* **65** 851–1112
[13] Madi C S, Davidovitch B, George H B, Norris S A, Brenner M P and Aziz M J 2008 *Phys. Rev. Lett.* **101** 246102
[14] Ozaydin G, Ludwig K F, Zhou H and Headrick R L 2008 *J. Vac. Sci. Technol.* B **26** 551–8
[15] Ziberi B, Frost F, Tartz M, Neumann H and Rauschenbach B 2008 *Appl. Phys. Lett.* **92** 063102
[16] Sánchez-García J A, Vázquez L, Gago R, Redondo-Cubero A, Albella J M and Czigány Z 2008 *Nanotechnology* **19** 355306
[17] Bock W, Gnaser H and Oechsner H 1993 *Surf. Sci.* **282** 333–41
[18] George H B 2007 Ion-stimulated mass transport in nanoscale morphology evolution *PhD Thesis* Harvard University
[19] Gago R, Vázquez L, Plantevin O, Sánchez-García J A, Varela M, Ballesteros M C, Albella J M and Metzger T H 2006 *Phys. Rev.* B **73** 155414
[20] Zhou H, Wang Y, Zhou L, Headrick R L, Ozcan A S, Wang Y, Ozaydin G and Ludwig K F 2007 *Phys. Rev.* B **75** 155416
[21] Sigmund P 1973 *J. Mater. Sci.* **8** 1545–53
[22] Facsko S, Bobek T, Stahl A, Kurz H and Dekorsy T 2004 *Phys. Rev.* B **69** 153412
[23] Vogel S and Linz S J 2006 *Europhys. Lett.* **76** 884–90
[24] Brown A D and Erlebacher J 2005 *Phys. Rev.* B **72** 075350
[25] Asaro R J and Tiller W A 1972 *Metall. Trans.* **3** 1789–96
[26] Spencer B J, Voorhees P W and Davis S H 1993 *J. Appl. Phys.* **73** 4955–70
[27] Kalyanasundaram N, Moore M C, Freund J B and Johnson H T 2006 *Acta Mater.* **54** 483–91
[28] Ozaydin G, Ludwig K F, Zhou H and Headrick R L 2008 unpublished
[29] Madi C S, George H B and Aziz M J 2008 unpublished